FORMATION ATTITUDE OPTIMIZATION WITH A MULTI-IMPULSE DESIGN*

Aaron B. Hoskins and Ella M. Atkins
University of Maryland Space Systems Lab
College Park, MD 20742

ABSTRACT

The proposed Magnetospheric Multi-scale (MMS) formation flight mission requires regular tetrahedron geometry as it follows a highly eccentric orbit through the Earth's magnetosphere, but formation attitude is not constrained. Due to potential corruption of the local magnetic field with particles output by satellite thrusters, we examine a mission design in which multiple impulses per orbit are used to maximize tetrahedron quality with minimal disruption to data acquisition. This paper extends previous efforts by optimizing MMS over formation (tetrahedron) attitude as well as position relative to a reference orbit. Candidate solutions are checked to ensure satellites do not collide. The effects of perturbations on formation quality, fuel use, and drift away from the Keplerian orbit are analyzed. This paper also presents an iterative Lambert's method that enables optimization over perturbed dynamics and compares perturbed results with the original Keplerian solutions.

INTRODUCTION

Spacecraft formation flight will reduce production and launch costs while increasing data collection capabilities. The proposed Magnetospheric Multi-scale (MMS) formation flight mission requires a tetrahedron geometry as it follows a highly eccentric orbit through the Earth's magnetosphere, but the formation is not required to have a specific attitude as it acquires data. Single-satellite and formation missions have traditionally been designed with natural orbit solutions that require infrequent correction. More recently, formations have been designed using a virtual structure/virtual rigid body (VRB)[1,2] representation that utilizes active control to maintain precise geometries. With such a representation, each spacecraft acts as a "node" in an overall formation "structure" held together by natural and active control forces rather than by rigid physical components. In previous work,[2] a VRB design was proposed for the MMS mission such that the formation actively maintained perfect geometry with reasonable fuel usage over a specific region of each orbit, designated by width $\Delta\nu$ and center position ν_c as shown in Figure 1. Due to the corruption of the local magnetic field with particles output by satellite thrusters, a series of solutions have subsequently been investigated[3] in which multiple impulses per orbit are used to improve tetrahedron quality with minimal disruption to data acquisition. This paper extends previous efforts by optimizing MMS over formation (tetrahedron) attitude as well as position relative to a reference orbit, and examines the effects of perturbation forces both on Keplerian-optimal solutions and on design parameters optimized over the perturbed system. Due to the substantial search-space size, a particle swarm optimization (PSO) technique is utilized.

Our multi-impulse solution was derived from a hybrid VRB-natural orbit design, as shown in Figure 1, where the shaded area $\Delta\nu$ depicts the actively controlled region in which tetrahedron geometry is maintained perfectly as a VRB. The VRB uses three reference frames to define spacecraft positions. The target reference orbit (**T**-frame) is defined by a set of orbital elements (semi-major axis a, eccentricity e, inclination i, right ascension of the ascending node Ω, argument of periapsis ω, and true anomaly ν). The design investigated for this paper utilizes an equatorial orbit, so Ω and ω are combined as the true longitude of periapsis $\tilde{\omega}_{true}$. The origin of the virtual vehicle frame (**V**-frame) is offset (V_x, V_y, V_z) from the **T**-frame. Both **V** and **T** are defined relative to an Earth-centered, inertial coordinate frame. The position of each formation spacecraft k is defined by frame $\mathbf{D_k}$ relative to the **V**-frame.

Our baseline design (with a default formation attitude)[3] was optimized over design vector ($\Delta\nu$, ν_c, $\tilde{\omega}_{true}$, V_x, V_y, and V_z). To optimize formation attitude, we have included six additional design variables representing Euler x-y-z formation orientations at the two orbital stations where burns are applied (P_1 and P_2). $\tilde{\omega}_{true}$ was removed from the

* This work was partially supported under NASA GSFC Grant NNG04GA64A.

search space because it was redundant with the Euler z-axis rotation. Representative orbital elements for the reference **T**-frame were defined based on MMS requirements[4] and were presumed the same for each optimization result to be presented: a=61,230.144 km, e=0.875, i=0°, and $\tilde{\omega}_{true}$=0°.

Due to symmetries given tetrahedral geometry and identical satellites, design parameters Δν and ν_c were investigated over the range 0°-180°, and the six Euler angles specifying attitude were bounded to ±30°. All design problems presume the satellites start in a perfect tetrahedron configuration at orbital station P_1 with the same velocity as the **T**-frame. The satellites arrive at P_2 in a perfect tetrahedron with the selected formation attitude. Lambert's method is used to calculate the required impulses for each satellite, and the satellites are not controlled during transits between P_1 and P_2. The same methodology is used to calculate the Δν's for the satellites to perfectly reassemble at P_1 in their original configuration after leaving P_2. Equation (1) shows the cost function over which the formation is optimized:

$$J = w_1\left(\sum_{Q_{R,i}\geq Q_{R,\min}} Q_{R,i}\cdot\Delta t\right) + w_2\left(\frac{\Delta v}{T_{obs}}\right) \tag{1}$$

where w_1 and w_2 are weighting factors, $Q_{R,min}$, is the minimum acceptable values of Robert-Roux quality factor Q_R, ($Q_{R,i}$) is Q_R at station i in the orbit, Δt is the orbit propagation time step, Δv is the total Δv applied around the orbit, and T_{obs} is the total time of observation per orbit. Our current weight set is w_1=-1 and w_2=1.3*10^{12}, a scaling that has been determined to generally balance fuel and quality factor influences. Note that w_1 is negative because quality factor is maximized while the cost function is minimized.

After a discussion of the two-body results, perturbations are considered. Previous research has investigated the long-term influence perturbations can have on a mission[5] while other research has investigated the creation of a state transition matrix that includes J2[6]. Linearized equations of motion that include J2 have been developed[7]. However, the orbit investigated for this research has high altitude and high eccentricity, so inclusion of additional perturbing forces is required to achieve an accurate solution. We present an algorithm embedded within our PSO process that utilizes Lambert's method in conjunction with a Simplified Deep Space Generalized Perturbations (SDP) model to enable optimization over a more complete set of forces.

TWO-BODY RESULTS

We have applied a particle swarm optimization (PSO) algorithm for MMS to enable rapid exploration over the space of design variables[3]. For the Keplerian model, over 574 PSO runs the best solution had $\Delta\nu$=0.4567 rad, ν_c=3.0944 rad, **V** = [1.1217, -16.0349, -99.9574] km and XYZ Euler orientations [0.1793, -0.1516, 0.3045] rad for P_1 and [-0.4066, 0.3174, 0.2880] rad for P_2. The **V** offset vector, in combination with the respective rotation set, defines the offset from the **T**-frame at P_1 and P_2. Formation geometry snapshots at P_1 and P_2 as well as apogee and perigee are illustrated in Figure 2. Our optimal solution indicates close proximity to the **T**-frame x-axis is more critical than for y and z. Because the semi-major axis of the **T**-frame is coincident with the x-axis, it is logical that distance from the x-axis should be minimized since separation from the **T**-frame x-axis causes a change in natural orbital period that must be corrected. This same trend was observed with the optimal solution to the default formation attitude problem; Reference 3 provides a more detailed explanation. The result indicated a linear relationship between V_x and V_y as shown in Figure 3.

The inclusion of formation attitude in our design vector has decreased solution cost compared with previous results; the default formation attitude solution[3] had a total cost of -1.07*10^5 using Equation (1) with w_1=-1 and w_2=1.3*10^{12}. The attitude-optimal solution has total cost –1.15*10^5 using the same cost function weights, a 9% decrease in cost. The total Δv summed over all satellites is 8.63*10^{-4} km/sec per orbit for the attitude-optimal solution, a 12% decrease relative to the default formation attitude solution. Table 1 summarizes the default formation attitude and attitude-optimal results, while Figure 4 provides a comparison of quality factor Q_R over a full orbit. Note that although quality factor for our new solution is less than default formation attitude quality for an interval after *P2*, optimizing over attitude has improved quality around apogee where data would mostly likely be collected. In summary, the attitude-optimal solution has improved the default attitude solution with respect to both quality and required fuel expenditure.

To study the nature of the minima, we exploit the fact that PSO, like other evolutionary algorithms, cannot guarantee that the globally best solution is always found.

Table 2 summaries the set of 153 candidate solutions near the apparent global minima (cost ≤ 1.15 * 10^5) identified for the 488 PSO optimization processes. The selection of Δv, ν_c, and V_z has been previously explained[3].

$\Delta\nu$ is selected to allow the two burns to occur near apoapsis. The exact value determines how low the quality factor will be at apoapsis. ν_c centers P_1 and P_2 approximately about apoapsis. The slope of the line in Figure 3 is 135º greater than the flight path angle at P_2. The offset of the line changes signs when the sign of the *z* rotation angle changes due to the change in the roles of satellites 2 and 3. V_y and V_z appear randomly distributed as shown in Figure 5; however the value of V_x does appear to depend on the value of V_y. All Euler angle rotations were searched over an interval $\pm$ 0.5236 radians ($\pm$ 30°), so we conclude the

Table 2 values were not influenced by search-space boundaries. P_1 and P_2 have noticeably different formation attitudes. For a positive *z* rotation at *P1*, satellite 3 is rotated so that its unit vector is primarily along the **V**-frame *x*-axis. Satellites 1 and 4 have the same basic relationship with the *y*- and *z*-axes respectfully. Because of the geometry, and the other three satellites' proximity to the axes, satellite 2 is approximately equidistant from the *x*- and *y*-axes; it is also the only one of the four satellites with a negative *z* component. The rotation of the formation about the *z*-axis is approximately equal at both orbital stations. The relationship between optimal angle values is best seen in graphical form. As shown in Figure 6, the *z*-axis rotation at P_1 is close to equal to the *z*-axis rotation at P_2. The few negative rotation solutions are near the search space boundary and are removed from the data set for analysis. Figure 3 showed that the offset of a line fitting the data can change when the sign of the rotation changes. A best-fit solution for the data in Figure 3 is the line perpendicular to the two lines that can be drawn through the two data sets. For this reason and the fact that boundary data is more likely to be a local minimum, we focus analysis on positive *z* rotation solutions. The rotation about the *z*-axis effectively causes a change in the value of $\tilde{\omega}_{true}$ for the transfer orbit. A node change at the burn site would increase the amount of needed fuel.

Figure 7 and Figure 8 illustrate the rotation angles at P_1 and P_2 respectfully for the candidate solutions close (within 0.15%) to the best solution. Two clusters appear in the plots because of the symmetry of the formation. If the bounds of the search space were altered slightly, then the cluster in the negative *z* region of the plots would be found at in the positive *z* region. The transit from P_1 to P_2 is near apogee and the satellites are moving relatively slowly compared with their orbital speed. As can be seen in Figure 9, the rotation specified at P_1 for the lowest cost solution aligns the formation more closely with the motion of the target orbit. By rotating the formation so that it is more closely aligned with the path of the target orbit, the quality factor increases since the satellite orbits are more similar.

In comparison, the transition from P_2 to P_1 will not provide as good an opportunity to collect data because even slight differences in satellite orbits will cause the formation to degrade significantly given the high orbit velocities near perigee. Because quality factor and observation time will be insignificant, the dominant cost function term for the P_2- P_1 transit is fuel. If a satellite is on the target orbit, it incurs minimal fuel cost because it will naturally arrive at P_1 with the same velocity as the target frame. It is not possible to place all four satellites on the target orbit and have a quality factor of one at P_2 (or P_1). However, the rotations at P_2, as can be seen in Figure 10, place the three in-plane satellites approximately on the target orbit thereby minimizing fuel cost.

As illustrated by the Figure 2 perigee plot, formation satellites may travel quite close to each other over the drift orbit. We incorporated a collision avoidance check in our optimization process to eliminate any solution that is infeasible due to potential satellite collision. However, by removing solutions with collision potential, PSO clustering/convergence performance was reduced. Because PSO convergence degraded with the inclusion of a collision check, it was removed from the optimization process. However, as can be seen in Figure 11, post-processing of the optimal solution determined that the closest approach of any two satellites in our lowest-cost solution is greater than 1.25 km. We have elected to post-process the final solution and if a future solution is found in which a collision might occur, then the optimization will be rerun including the collision check. This procedure allows PSO to perform efficiently but still guarantee that our final solution will be collision-free.

We also post-processed our solution to examine the influence of perturbations so that a more realistic assessment of our MMS design can be made. Perturbations due to the moon, atmospheric drag, and the J_2-J_5 forces were all included in the numerically integrated simulation[8]. The velocities determined using Lambert's method were applied to the satellites at P_1 and P_2. To reduce the position and velocity error, a local iteration scheme[3] targeting the Keplerian-optimal solution was first employed. In summary, this procedure first propagated the formation from P_1 to P_2. Next, the position error was calculated at P_2 and Lambert's method was used to determine the orbit that passed through P_1 and P_2 minus the error vector. The formation was then propagated again from P_1, but now used P_1 velocity required to pass through the offset P_2 location. As with the default formation attitude solution, there was an increase of needed fuel when perturbations were included; this is to be expected because fuel must be used to compensate for the disturbances.

Table 3 shows the position error and the Δv of the satellites after the iteration scheme; by comparing the perturbed results with the two-body results (Table 1), it can be seen that each satellite needs significantly more fuel at both P_1 and P_2 than when the entire mission was modeled with only two-body forces. These results suggest that

the perturbing forces should be considered during the optimization process, since the order of magnitude increase in fuel given perturbations dominates the total fuel required for the Keplerian-optimal result.

PERTURBED TWO-POINT BOUNDARY PROBLEM WITH FIXED TIME

Table 3, the Keplerian-optimal solution is likely not the optimal design given realistic perturbations. Previous research has introduced algorithms for solving Lambert's problem with J2[9] and also for J2 through J6[10]. However, the apogee radius of our orbit is approximately 116,000 km (~18 ER), so third body perturbations are also significant.

The simulator we used for the above post-processing analysis numerically integrates the satellite location at each time step. Using the iterative method developed to reduce the position error required approximately 15 minutes on a 3 GHz machine. The optimization method, as it was implemented, required 40 solutions per iteration and potentially 15,000 iterations. At this rate, a single data run would complete in roughly 15 years, thus it is not realistic to include the numeric simulator in our optimization process.

Software that approximates perturbing forces based on analytical methods was identified to include these effects in our initial optimization while maintaining reasonable computational complexity. The SGP library functions[11] were selected, specifically the SDP4 routine because our target orbit period is greater than the 225-minute boundary suggested between the use of SGP4 and SDP4. The input to SDP4 is intended to be two-line element data files, so mean elements rather than osculating elements are required. As a simplification, we assume that B^*, $\dot{n}$, and $\ddot{n}$ are equal to zero. To calculate the osculating elements, we use the velocity determined using a two-body Lambert method. Then to calculate the mean elements needed by SDP4, we assume that the osculating elements at the start of the transfer are the same as the mean elements. We know that this assumption is not fully accurate, but it provides an initial estimate of the actual solution. The use of osculating elements introduces error in both the initial and final positions, and a procedure was needed to identify the mean elements that define an orbit which passes through the two desired locations separated by a specified amount of time.

Equation 2 is used to calculate the error between the desired positions and the calculated positions. SDP4 is used to propagate the orbit to P_1 and P_2.

$$d\vec{r} = \vec{r}_d - \vec{r}_c \tag{2}$$

where $d\vec{r}$ is the error vector, $\vec{r}_d$ is the desired position vector, and $\vec{r}_c$ is the calculated position.

The next step is to calculate a matrix of the derivatives, computed numerically in this work. Each orbital element was varied a small amount while the others were held at the values determined during the previous iteration, and SDP4 was called with the slightly altered element set. The error vectors for both the initial and final locations due to the slight change in the orbital elements were calculated. The resulting vectors were divided by the change in the particular orbital element. After 12 calls of SDP4 (six elements computed at position vectors P_1 and P_2), the matrix in Equation 3 is fully populated.

$$A = \begin{bmatrix} \frac{\partial x_i}{\partial n} & \frac{\partial x_i}{\partial e} & \frac{\partial x_i}{\partial i} & \frac{\partial x_i}{\partial \Omega} & \frac{\partial x_i}{\partial \omega} & \frac{\partial x_i}{\partial M} \\ \frac{\partial y_i}{\partial n} & \frac{\partial y_i}{\partial e} & \frac{\partial y_i}{\partial i} & \frac{\partial y_i}{\partial \Omega} & \frac{\partial y_i}{\partial \omega} & \frac{\partial y_i}{\partial M} \\ \frac{\partial z_i}{\partial n} & \frac{\partial z_i}{\partial e} & \frac{\partial z_i}{\partial i} & \frac{\partial z_i}{\partial \Omega} & \frac{\partial z_i}{\partial \omega} & \frac{\partial z_i}{\partial M} \\ \frac{\partial x_f}{\partial n} & \frac{\partial x_f}{\partial e} & \frac{\partial x_f}{\partial i} & \frac{\partial x_f}{\partial \Omega} & \frac{\partial x_f}{\partial \omega} & \frac{\partial x_f}{\partial M} \\ \frac{\partial y_f}{\partial n} & \frac{\partial y_f}{\partial e} & \frac{\partial y_f}{\partial i} & \frac{\partial y_f}{\partial \Omega} & \frac{\partial y_f}{\partial \omega} & \frac{\partial y_f}{\partial M} \\ \frac{\partial z_f}{\partial n} & \frac{\partial z_f}{\partial e} & \frac{\partial z_f}{\partial i} & \frac{\partial z_f}{\partial \Omega} & \frac{\partial z_f}{\partial \omega} & \frac{\partial z_f}{\partial M} \end{bmatrix} \tag{3}$$

where x, y, and z are the components of the error vector, i and f differentiate the initial and final positions, and the orbital elements are mentioned above.

A computationally efficient way to iterate the orbital elements is via Equation 4.

$$\vec{k}_{j+1} = \vec{k}_j - A^{-1}\vec{k}_j \tag{4}$$

where $\vec{k}$ is the vector of orbital elements and j is the iteration number. However, this method is not guaranteed to converge on a solution. If it has not converged to within 1 m of total error within 1000 iterations, then a nonlinear least squares method is tried using the solution with the least total error as the initial guess of the solution. It is more

computationally expensive, but it has shown to converge in instances when the previous method did not. The same *A* matrix is created for this method as well, but instead of using Equation 4 to calculate the new orbital elements, the next step is to create a six element column vector of the amount of position error (Equation 5) and then solve Equation 6.

$$\tilde{b} = \begin{bmatrix} d\vec{r}_i \\ d\vec{r}_f \end{bmatrix} \tag{5}$$

$$\begin{bmatrix} \Delta n \\ \Delta e \\ \Delta i \\ \Delta\Omega \\ \Delta\omega \\ \Delta M \end{bmatrix} = \left(A^T A\right)^{-1} A^T \tilde{b} \tag{6}$$

This method is allowed to iterate up to 1000 times as well. However, the use of the forward differencing approach did not always converge on a solution that met our required one-meter total error metric. There were also instances when the process diverged to a hyperbolic orbit causing the process to terminate. To ensure convergence, we have also included a Nelder-Meade optimization function from the GNU Scientific Library (GSL) to find a solution that minimizes total distance error. If these three processes are unable to find a solution, we use a PSO algorithm. The three previous methods do not always improve the best solution that has been found; however the PSO algorithm finds a better solution more than 99% of the time. However, these four methods do not always reduce the error to our one-meter standard. As a result, the four methods are executed iteratively until a solution with the one-meter error standard is returned. For the first satellite, the initial guess is the two-body Lambert solution. The initial guess for the Nelder-Meade and PSO is the best solution that has been found. The initial guess for satellites 2-4 is the solution of the previous satellites. Because the satellites are separated by 10 kilometers, the four solutions are relatively close to each other, so it saves computation time to start with a guess that is closer to the actual solution than the two-body Lambert solution. This iterative process is potentially too time consuming to be used to solve the inner optimization to one-meter accuracy; however it can be used as a post-processing step to examine the influence of perturbations on our results.

In an attempt to include the effect of perturbations in our initial optimization, we incorporated SDP4 to calculate the locations of P_1 and P_2 by using the **T**-frame orbital elements as the mean elements passed into SDP4[†] with the mean anomaly value that corresponded to a ν value of ν_c-$\Delta\nu$/2. The orbit was then propagated to a time of 0 seconds and the time that it would take to go ν_c radians from P_1. The final state was determined by using SDP4 to calculate the state one period later based on a. Using this software design to post-process our Keplerian-optimal solution provided comparable results to those produced by numerical integration with perturbations, but this method was comparable in speed to our two-body method. As a result, we used this method as part of the optimization process. This "perturbed **T**-frame" optimization process found a solution that used an order of magnitude more fuel than the Keplerian-optimal solution and had little observation time. Substantially less fuel was required, but the results were not promising for an actual mission. As shown in

Table 4, the optimal result found using this method requires a significant amount of fuel and has very little observation time.

Instead of using the optimal result returned by the "perturbed **T**-frame" method, we returned to the Keplerian optimal solution for further analysis. The two perturbation methods (numerically integrating forces and perturbing the **T**-frame) both require more fuel because of the same basic flaw. The Keplerian-optimal solution determined transfer orbits based on two-body dynamics to have a tetrahedron formation of satellites follow a virtual satellite whose motion was calculated based on two-body dynamics. The numerical integration approach attempted to match a perturbed formation with a virtual satellite based on two-body motion. The perturbed **T**-frame attempted to match a two-body dynamics formation with a perturbed virtual satellite. The difference in force models used on the two components of the system was the cause of a majority of the increased fuel cost. Because of this fact, we used our perturbed Lambert's method with a perturbed **T**-frame to post-process the Keplerian-optimal solution.

Table 4 includes a comparison of these results with those from the previously discussed methods. There is an increase in the amount of fuel when both the **T**-frame and satellites' orbits are perturbed (a factor of 4.6), but not nearly as significant an increase as with the perturbations of only the satellites' orbits (a factor of about 28). The

[†] The inclination of the **T**-frame is 0 radians, but there is a singularity in the SDP4 code at 0 radians, so a value of 10^{-10} was used to avoid numerical problems.

quality factor was calculated using two-body propagation and it is possible that the quality factor and observation time would improve if SDP4 is used to propagate the satellites. For the transit from *P1* to *P2*, the quality factor is virtually identical for the Keplerian optimal result and the result with perturbed **T**-frame and satellite orbits. The perturbed result decreases in quality much more rapidly after P_2. This behavior can be partially attributed to the fact that the use of osculating elements as the mean elements of the **T**-frame causes P_2 to be closer to periapsis.

CONCLUSIONS AND FUTURE WORK

We have investigated multi-impulse mission designs for a tetrahedron formation optimized over attitude as well as thrust application sites and offset from a reference orbit. The results show an improvement in cost (quality of observation, amount of fuel, and observation time) for the two-body solution over previous solutions presuming a fixed formation attitude at impulse application sites. Perturbations influence the cost of the final solution, but if all satellites, real and virtual, are controlled by the same dynamics, then the increase in cost due to perturbations is reasonable (~46%). To include perturbations in the general optimization process, analytical methods must be used in order for computation time to be manageable. These methods are not as exact as numerical integration, but provide a reasonable estimate. Future work will be spent on developing a perturbed Lambert's method that will reliably converge on the correct solution.

One of the assumptions made for this work is that a single orbit is repeated. However, the method we have implemented to include perturbations does not guarantee the formation will precisely return to P_1 for reassembly. In fact, the perturbing forces change for each orbit, so it is not likely to find an exact repeatable orbit that meets the mission requirements. We could use our perturbed Lambert's algorithm to find an orbit that passes through P_1 twice separated by the desired orbital period. P_2 would be calculated the same way as it is currently for the perturbed case: the time would be calculated based on two-body dynamics and then the orbit would be propagated over that time.

Convergence of the perturbed Lambert's method may be improved with a central-differencing approach rather than a forward differencing approach. The amount orbital elements are perturbed to create the **A** matrix does influence the convergence behavior. However the behavior is dependent on the particular orbit being analyzed. A quasi-Newton method that approximated the Hessian therefore could be more likely to reliably converge in a reasonable time. The optimal formation attitude results indicated that locations P_1 and P_2 serve different roles and therefore have different optimal formation attitudes. The optimal values of V_x, V_y, and V_z could be different at the two locations, so a logical next step would be to include a second set of offsets in the optimization process. This work has demonstrated that inclusion of formation attitude in the optimization process can in fact reduce overall mission cost. The inclusion of perturbing forces provides a more realistic evaluation for potential missions and the development of a perturbed Lambert's method that uses analytic methods rather than numerical integration could ultimately provide a general computationally inexpensive means to calculate the solution of a perturbed two-point fixed-time boundary value problem.

REFERENCES

1. Penneçot, Y., Atkins, E., and Sanner, R., "Intelligent Spacecraft Formation Management and Path Planning," *Proceedings of the AIAA Aerospace Sciences Conference*, Reno, Nevada, January 2002 (AIAA 2002-1072).
2. Chavez-Clemente, D. and Atkins, E., "Optimization of Tetrahedral Satellite Formations," *AIAA Journal of Spacecraft and Rockets*, vol. 42, no. 5, July-August 2005, pp. 699-710.
3. Hoskins, A. and Atkins, E., "Spacecraft Formation Optimization with a Multi-Impulse Design", to appear in *Proceedings of the AIAA Guidance, Navigation, and Control Conference*, San Francisco, California, August 2005.
4. Hughes, S. P., "Orbit Design for Phase I and II of the Magnetospheric Multiscale Mission", *Proc. AAS 27th Rocky Mountain Guidance and Control Conference*, Breckenridge, Colorado, February 2004.
5. Williams, Trevor; Register, Justin & Slater, Gary, "Formation-Keeping Maneuver Dispersions and Safe Mode Insertion for Satellite Formation Flight", *Proceedings of the AIAA Guidance, Navigation and Control Conference and Exhibit*, Providence, Rhode Island, August 2004 (AIAA 2004 – 4734)
6. Gim, Dong-Woo & Alfriend, Kyle T., "The State Transition Matrix of Relative Motion for the Perturbed Non-Circular Reference Orbit", *Proceedings of the AAS/AIAA Space Flight Mechanics Meeting*, Santa Barbara, California, February 2001, (AAS 01-222)
7. Schweighart, Samuel A. & Sedwick Raymond J., "High-Fidelity Linearized J2 Model for Satellite Formation Flight", *Journal of Guidance, Control, and Dynamics*, Vol. 25, No. 6, November-December 2002, pp. 1073-1080

8. Sanner, R. M., "*SATCON Distribute Satellite Formation Simulation and Control Code*," Space Systems Lab Technical Report (in progress), Aerospace Engineering Department, University of Maryland, College Park, Maryland.
9. Engles. R.C. and Junkins, J.L., "The Gravity-Perturbed Lambert Problem: A KS Variation of Parameters Approach", *Celestial Mechanics*, vol 24, pp. 3-21.
10. Wright, James R, "Solution to the Geocentric Lambert Boundary Value Problem for a Complete Force Field", *Proceedings of the AAS/AIAA Astrodynamics Conference*, Victoria, Canada August 1993, pp. 2611-2628.
11. Hoots, Felix R. and Roehrich, Ronald L., "SPACETRACK REPORT NO. 3: Models for Propagation of NORAD Element Sets", December 1980. (http://celestrak.com/NORAD/documentation/spacetrk.pdf).

Table 1: Comparison of Two-Body Default Formation Attitude and Attitude-Optimal Solutions

	Default Attitude	*Attitude-Optimal*
Cost	-1.07E+05	-1.15E+05
Total Δv (km/s)	9.83E-04	8.63E-04
Tobs %	82.2%	86.2%
Average Q	0.9440	0.9531

Table 2: Summary of Best Positive Z Rotation Results

	Max	*Min*	*Mean*	*Std*	*Std %*
Δv (rad)	0.4761	0.4251	0.4471	0.0111	0.704882
vc (rad)	3.1109	3.0752	3.0941	0.0078	0.4984334
Vx (km)	7.33	-4.00	1.37	2.96	2.963206
Vy (km)	99.64	-99.97	-10.92	59.38	59.38239
Vz (km)	100.00	-99.99	5.12	73.86	73.85836
P1 X Rotation (rad)	0.3976	-0.0157	0.2171	0.0981	18.739209
P1 Y Rotation (rad)	-0.0718	-0.2587	-0.1566	0.0421	8.0493373
P1 Z Rotation (rad)	0.5211	0.1165	0.2963	0.0962	18.373909
P2 X Rotation (rad)	-0.1956	-0.5226	-0.3536	0.0889	16.984152
P2 Y Rotation (rad)	0.4358	0.1771	0.3132	0.0517	9.8774351
P2 Z Rotation (rad)	0.4938	0.1548	0.2878	0.0789	15.061746

Table 3: Perturbation Error and Δv after Iteration for the Attitude-Optimal Solution

P1	*Δx (km)*	*Δy (km)*	*Δz (km)*	*Δr (km)*	*Δvx (km/s)*	*Δvy (km/s)*	*Δvz (km/s)*	*Δv (km/s)*	*Δv Kep-Opt (km/s)*
S1	-0.11	-1.67	-0.05	1.67	1.71E-03	2.04E-03	1.62E-04	2.67E-03	1.60E-11
S2	-1.38	-2.06	-0.09	2.48	1.82E-03	1.95E-03	1.63E-04	2.67E-03	1.04E-04
S3	-0.22	-1.63	-0.05	1.65	1.53E-03	2.26E-03	1.62E-04	2.74E-03	3.70E-04
S4	-0.22	-1.67	-0.07	1.68	1.72E-03	2.03E-03	1.62E-04	2.67E-03	9.05E-12
P2									
S1	0.03	0.01	0.00	0.04	3.21E-03	-8.98E-04	3.18E-04	3.35E-03	1.31E-11
S2	0.02	-0.02	0.01	0.03	3.31E-03	-8.31E-04	3.17E-04	3.43E-03	8.55E-05
S3	0.02	-0.01	-0.01	0.03	2.91E-03	-1.10E-03	3.18E-04	3.13E-03	3.03E-04
S4	0.02	0.02	0.03	0.04	3.21E-03	-8.97E-04	3.18E-04	3.35E-03	7.42E-12

Table 4: Summary of Different Methods

	Keplerian	*SDP4 for T-frame*	*Num. Int. of S/C*	*SDP4 for S/C*	*SDP4 for T-frame & S/C*
Cost	-1.15E+05	3.98E+07	9.81E+04	1.66E+05	-7.33E+04
Total Δv (km/s)	8.63E-04	7.65E-02	2.40E-02	2.61E-02	3.99E-03
Tobs %	86.2%	1.7%	90.8%	79.9%	80.9%
Average Q	0.9531	0.8393	0.9493	0.9536	0.9491
Selection of Varia	Optimized	Optimized	Kep. Solution	Kep. Solution	Kep. Solution

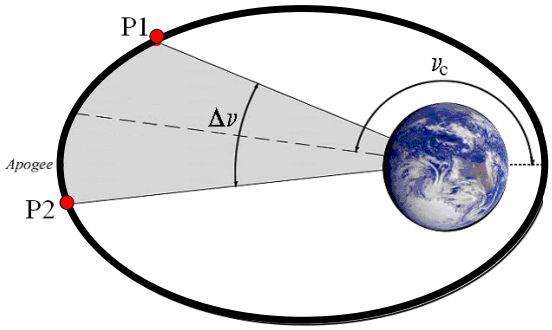

Figure 1. Impulsive Burn Orbital Stations

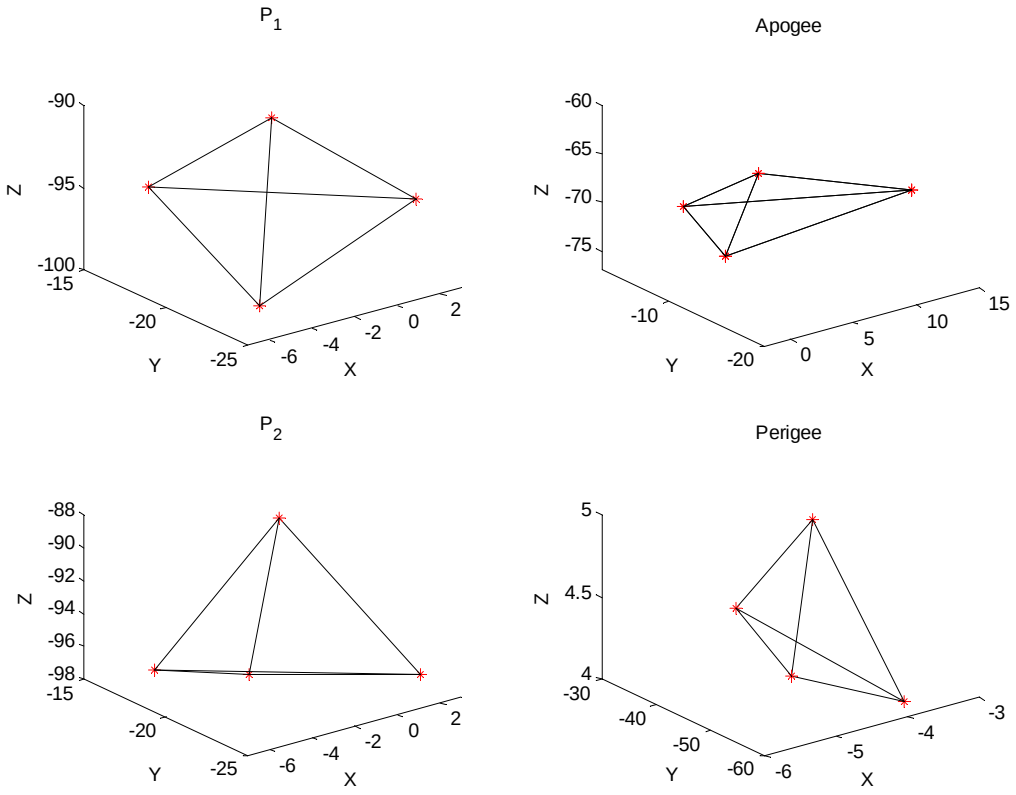

Figure 2. MMS Geometry at varied Orbital Stations

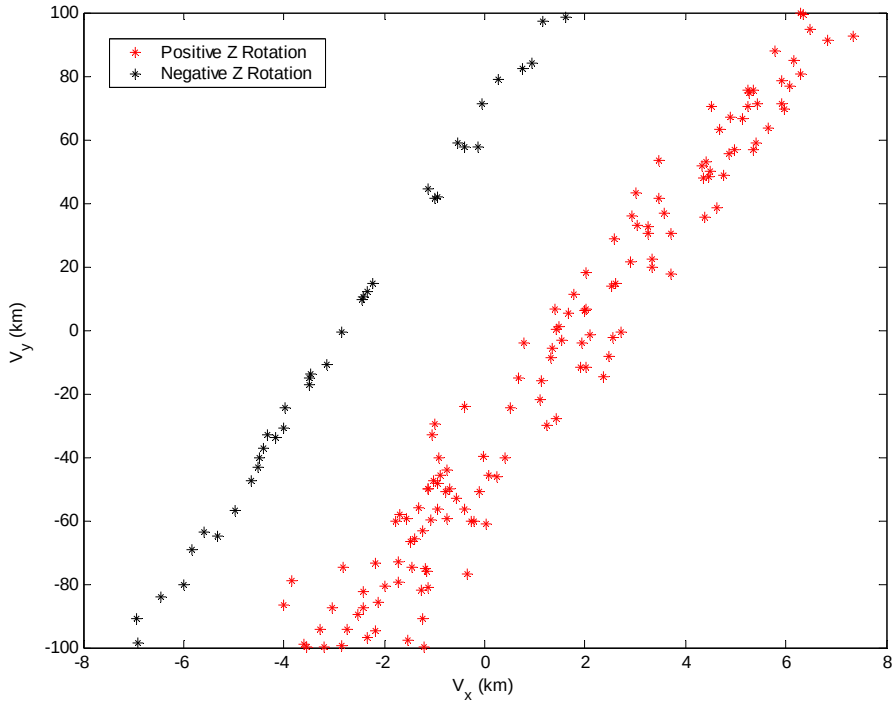

Figure 3. Vy vs. Vx

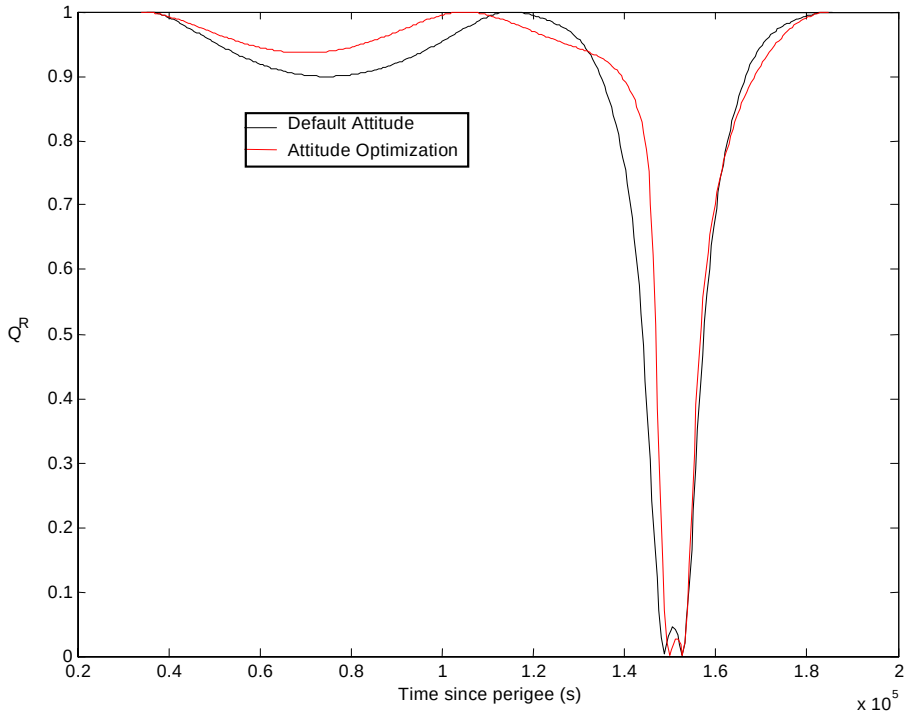

Figure 4. MMS Quality Evolution with and without Formation Attitude Optimization

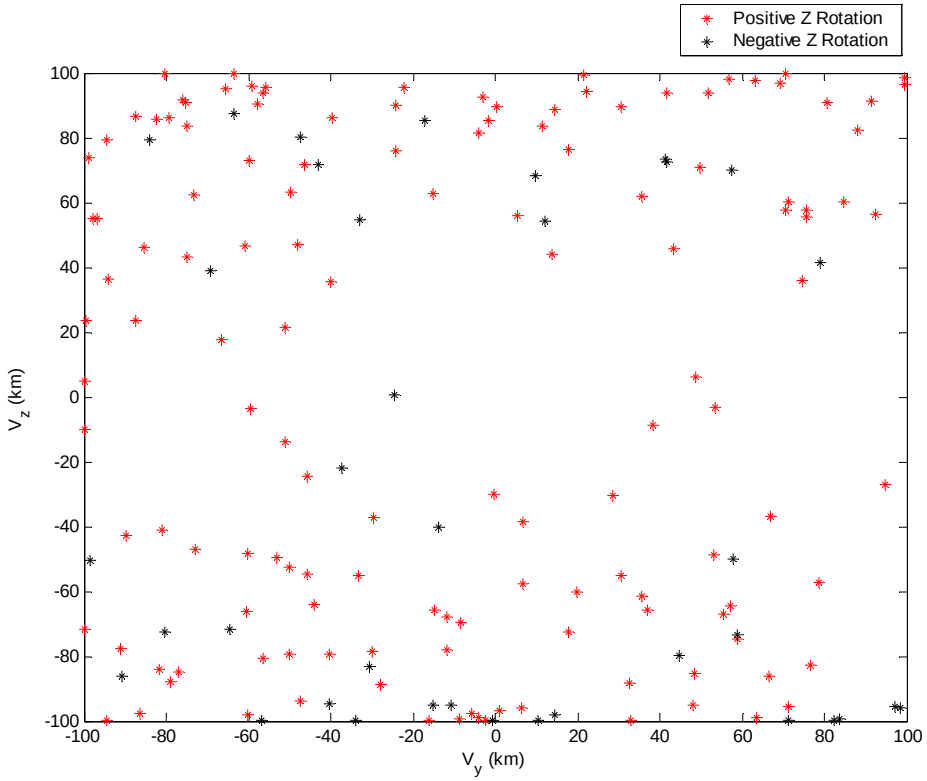

Figure 5. Vz vs. Vy

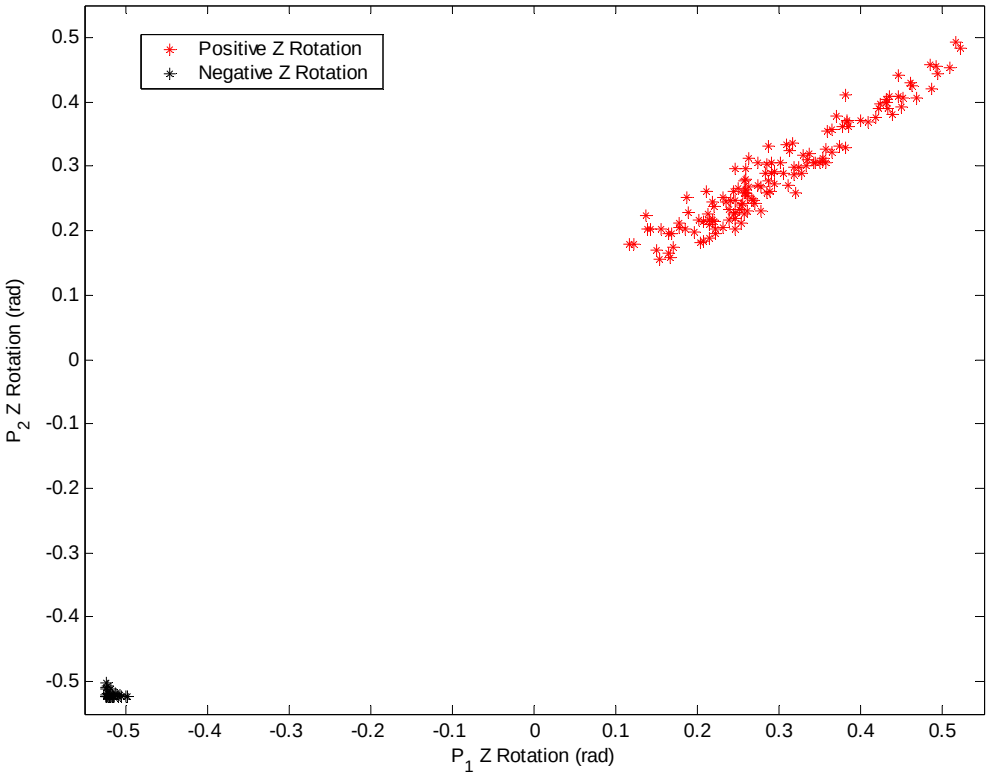

Figure 6. Relationship Between Z Rotations at P1 and P2

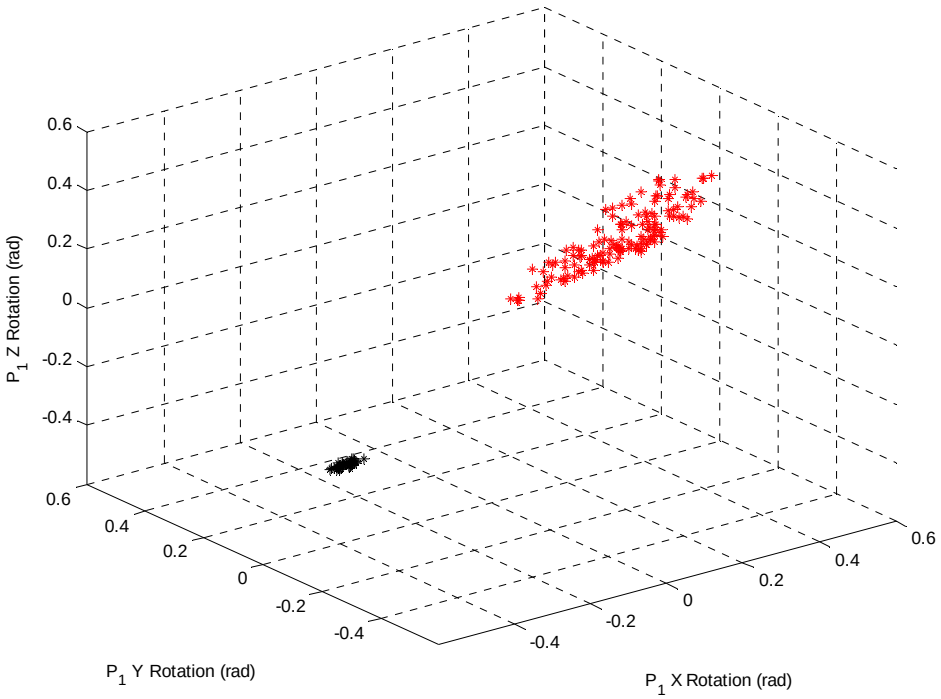

Figure 7. P1 Rotation Angles

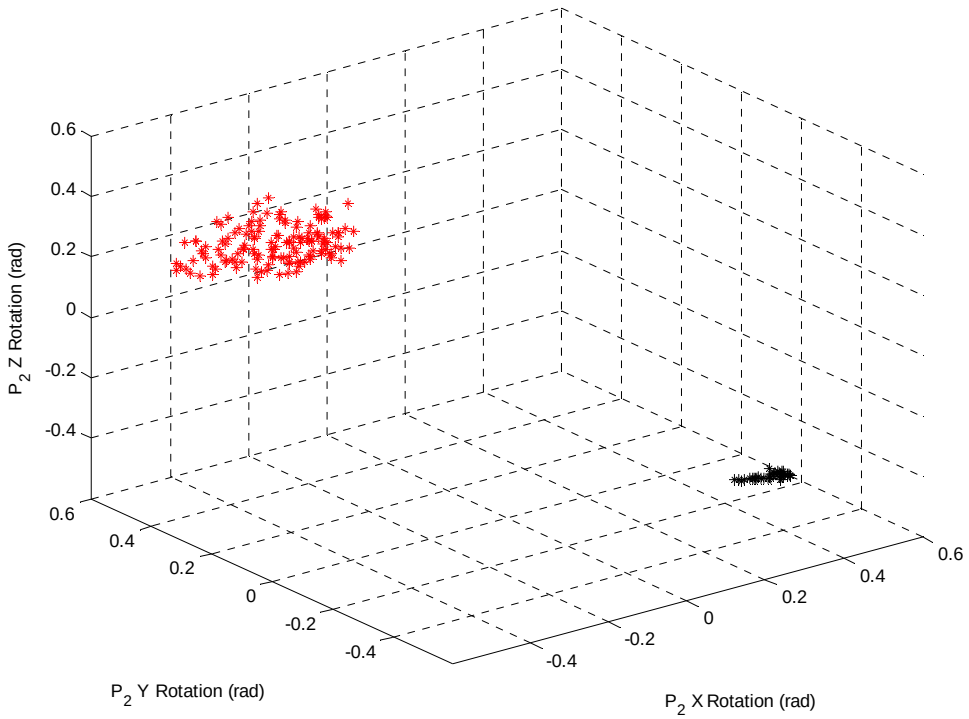

Figure 8. P2 Rotation Angles

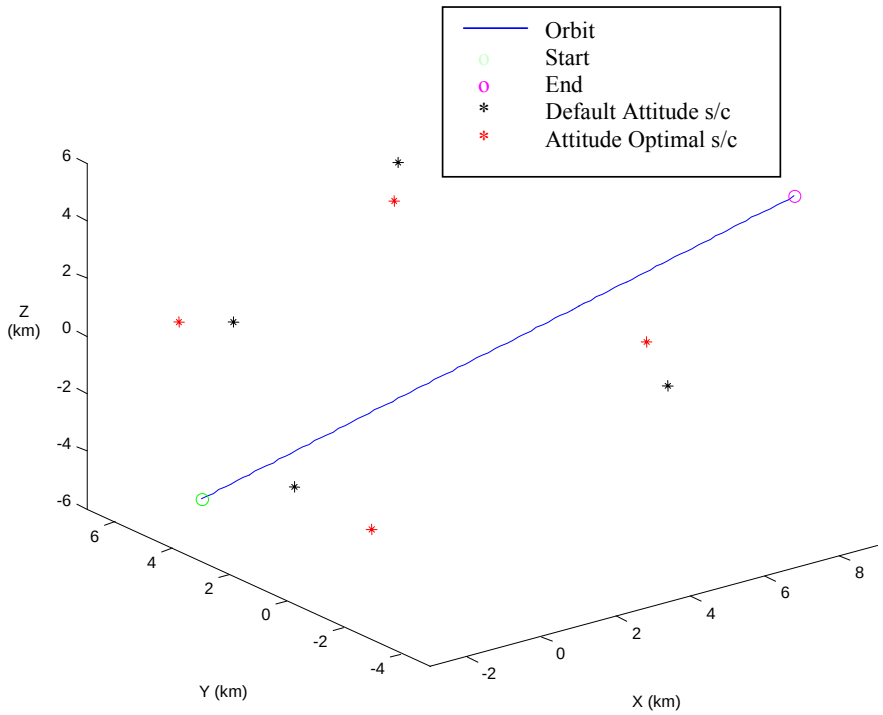

Figure 9. Formation at P1 for Attitude-optimal and Default Attitude Configurations (Distances in km)

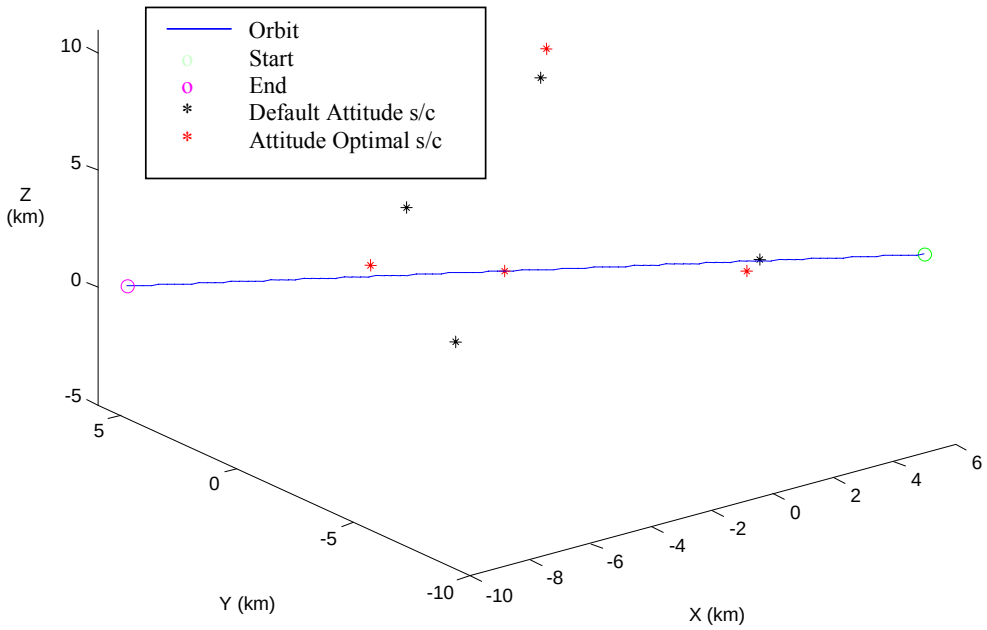

Figure 10. Formation at P2 for Attitude-optimal and Default Attitude Configurations (Distances in km)

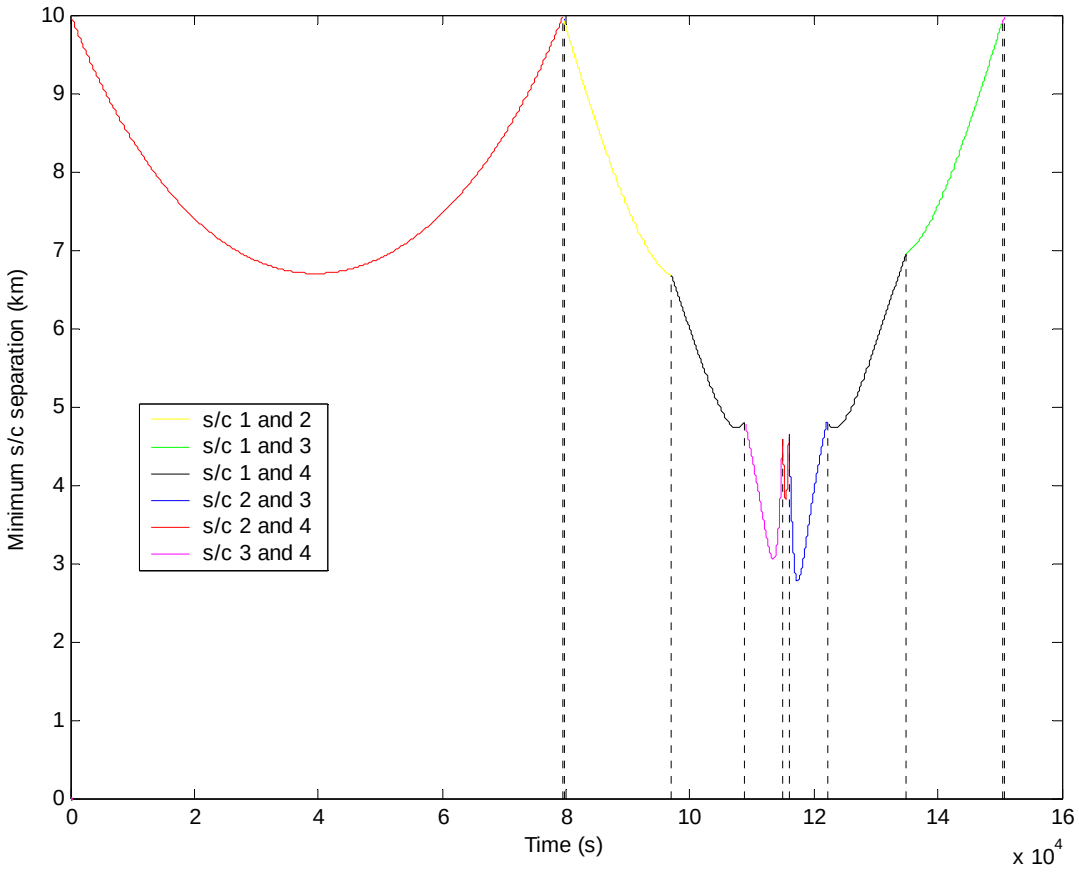

Figure 11. Minimum Spacecraft Separation for the Attitude-optimal Solution